Am J Physiol Heart Circ Physiol 316: H1167–H1177, 2019.
First published February 15, 2019; doi:10.1152/ajpheart.00319.2018.

RESEARCH ARTICLE | *Muscle Mechanics and Ventricular Function*

Pulmonary vascular mechanical consequences of ischemic heart failure and implications for right ventricular function

Jennifer L. Philip,[1,2] Thomas M. Murphy,[1] David A. Schreier,[1] Sydney Stevens,[4] Diana M. Tabima,[1] Margie Albrecht,[4] Andrea L. Frump,[4] Timothy A. Hacker,[3] Tim Lahm,[4,5,6] and Naomi C. Chesler[1,3]

[1]*Department of Biomedical Engineering, University of Wisconsin-Madison College of Engineering, Madison, Wisconsin;* [2]*Department of Surgery, University of Wisconsin-Madison, Madison, Wisconsin;* [3]*Department of Medicine, University of Wisconsin-Madison, Madison, Wisconsin;* [4]*Department of Medicine, Indiana University School of Medicine, Indianapolis, Indiana;* [5]*Department of Cellular and Integrative Physiology, Indiana University School of Medicine, Indianapolis, Indiana; and* [6]*Richard L. Roudebush Veterans Affairs Medical Center, Indianapolis, Indiana*

Submitted 23 May 2018; accepted in final form 10 February 2019

Philip JL, Murphy TM, Schreier DA, Stevens S, Tabima DM, Albrecht M, Frump AL, Hacker TA, Lahm T, Chesler NC. Pulmonary vascular mechanical consequences of ischemic heart failure and implications for right ventricular function. *Am J Physiol Heart Circ Physiol* 316: H1167–H1177, 2019. First published February 15, 2019; doi:10.1152/ajpheart.00319.2018.—Left heart failure (LHF) is the most common cause of pulmonary hypertension, which confers an increase in morbidity and mortality in this context. Pulmonary vascular resistance has prognostic value in LHF, but otherwise the mechanical consequences of LHF for the pulmonary vasculature and right ventricle (RV) remain unknown. We sought to investigate mechanical mechanisms of pulmonary vascular and RV dysfunction in a rodent model of LHF to address the knowledge gaps in understanding disease pathophysiology. LHF was created using a left anterior descending artery ligation to cause myocardial infarction (MI) in mice. Sham animals underwent thoracotomy alone. Echocardiography demonstrated increased left ventricle (LV) volumes and decreased ejection fraction at 4 wk post-MI that did not normalize by 12 wk post-MI. Elevation of LV diastolic pressure and RV systolic pressure at 12 wk post-MI demonstrated pulmonary hypertension (PH) due to LHF. There was increased pulmonary arterial elastance and pulmonary vascular resistance associated with perivascular fibrosis without other remodeling. There was also RV contractile dysfunction with a 35% decrease in RV end-systolic elastance and 66% decrease in ventricular-vascular coupling. In this model of PH due to LHF with reduced ejection fraction, pulmonary fibrosis contributes to increased RV afterload, and loss of RV contractility contributes to RV dysfunction. These are key pathologic features of human PH secondary to LHF. In the future, novel therapeutic strategies aimed at preventing pulmonary vascular mechanical changes and RV dysfunction in the context of LHF can be tested using this model.

NEW & NOTEWORTHY In this study, we investigate the mechanical consequences of left heart failure with reduced ejection fraction for the pulmonary vasculature and right ventricle. Using comprehensive functional analyses of the cardiopulmonary system in vivo and ex vivo, we demonstrate that pulmonary fibrosis contributes to increased RV afterload and loss of RV contractility contributes to RV dysfunction. Thus this model recapitulates key pathologic features of human pulmonary hypertension-left heart failure and offers a robust platform for future investigations.

Address for reprint requests and other correspondence: N. C. Chesler, Univ. of Wisconsin at Madison, 2146 Engineering Centers Bldg., 1550 Engineering Dr., Madison, WI 53706 (e-mail: naomi.chesler@wisc.edu).

heart failure; pulmonary vascular remodeling; right ventricle dysfunction; secondary pulmonary hypertension; ventricular-vascular coupling

INTRODUCTION

Left heart failure (LHF) impacts nearly 5.9 million adults and contributes to 1 out of every 9 deaths in the United States (51). The prevalence of pulmonary hypertension (PH) in LHF is as high as 60–80% (18, 42). PH due to left heart failure (PH-LHF) is the most common cause of PH and is associated with a high morbidity and mortality (24, 25, 28). Due to a lack of a well-characterized animal models and the limitations of human subject research, investigations into disease pathophysiology and progression have been limited and much of current understanding of the mechanisms of this disease remains speculative (28, 46, 63). Current clinical understanding is that PH-LHF begins as a passive process due to elevated left atrium filling pressures that increase pressures throughout the pulmonary vasculature. In its early stage, this pulmonary venous hypertension is termed isolated postcapillary PH (Ipc-PH) and is diagnosed by elevated mean pulmonary arterial pressure (mPAP) and pulmonary capillary wedge pressure with normal pulmonary vascular resistance (PVR) and diastolic pressure gradient. In contrast, combined post- and precapillary PH (Cpc-PH) is diagnosed when PVR or diastolic pressure gradient is increased in this setting and confers an additional increase in mortality (17, 50). Cpc-PH represents a spectrum of disease severity including a reactive state, which is reversible and responsive to vasodilators and thought to be primarily driven by pulmonary vasoconstriction, and a fixed state that is irreversible, unresponsive to pharmacological interventions, and thought to be characterized primarily by small vessel narrowing and wall thickening (14, 28, 75). Cpc-PH prevalence is between 12 and 20% in patients with LHF (17, 24). Both elevated pulmonary arterial pressure (PAP) and increased PVR are associated with decreased survival in LHF (17, 24). Despite this high clinical significance, there are no current therapies that target PH-LHF other than optimization of LHF and some limited adaptation of therapies for pulmonary arterial hypertension (PAH) (24, 25, 28).

PVR has prognostic value in PH-LHF (17, 24) but is typically calculated from PAP and left atrial pressure at a single flow rate (i.e., cardiac output), which provides a limited assessment of pulmonary vascular function (52). Mechanically, the pulmonary vasculature can be considered to provide resistance to steady flow as well as impedance to pulsatile flow. While the resistance depends on the flow rate, albeit nonlinearly, the impedance depends on flow rate as well as frequency (i.e., heart rate). Thus a comprehensive assessment of pulmonary vascular function should include multipoint pressure-flow relationships and impedance to flow at a range of frequencies (9, 23, 52). No studies have characterized mechanical pulmonary vascular function in these ways in PH-LHF (11). Similarly, few assessments of pulmonary vascular structure have been performed in this disease. Autopsies on patients with PH-LHF have shown evidence of medial hypertrophy and fibrosis in pulmonary arteries (12, 29), corroborated by large animal studies of pulmonary venous hypertension (40, 59, 66). Small animal studies have shown pulmonary fibrosis and endothelial dysfunction (2, 8, 33, 37, 56). These pulmonary vascular structure changes associate with increases in PAP or PVR, but the resulting structure-function correlations are limited because key aspects of function have not been measured.

Ultimately, changes in pulmonary vascular structure and function in PH-LHF increase RV afterload and result in impaired RV mechanical function, which itself is a powerful predictor of survival in LHF (10, 13, 18, 35, 60). Robust assessment of RV mechanical function including ventricular-vascular interactions requires right ventricular (RV) catheterization with pressure-volume loop analysis at varying preloads (71). Especially since RV mechanical function depends on LV mechanical function via intraventricular interactions (26), quantifying the mechanical progression of pulmonary vascular and RV dysfunction in PH-LHF is critical to understanding disease pathophysiology and developing novel therapies to prevent cardiopulmonary deterioration in response to LHF progression.

Here we sought to investigate the mechanical mechanisms of pulmonary vascular and RV dysfunction in a rodent model of PH-LHF. We further compare our pathophysiological findings to published data from PH-LHF patients to verify the ability of our rodent model to recapitulate critical aspects of the human disease.

METHODS

Myocardial infraction model. All animal procedures were approved by the University of Wisconsin-Madison Institutional Animal Care and Use Committee. Adult C57/Bl6 male mice (6–8 wk of age, 18–26 g) were randomly divided into two groups for myocardial infarction (MI) or sham surgery as previously described (39). Briefly, mice were initially anaesthetized with 5% isoflurane and maintained with 1–2% isoflurane throughout the procedure. A left thoracotomy was performed, and the left coronary artery was ligated at the point where it emerges past the tip of the left atrium. Sham animals underwent thoracotomy alone. Immediate operative survival was 70% in the MI group and 100% in the sham group, consistent with previous reports (39, 54). One group of MI ($n = 6$) and sham ($n = 9$) mice underwent serial echocardiography, performed at 4, 8, and 12 wk postsurgery, followed by terminal hemodynamic assessment via either right heart catheterization. A second group of MI ($n = 6$) and sham ($n = 5$) mice underwent isolated lung perfusion to assess the pulmonary vasculature biomechanics at 12 wk postsurgery. Experiments were conducted in an unbiased approached with adherence to the recently published PH preclinical research guidelines (4, 62). Power calculations were completed to determine appropriate group sizes; animals were randomized to either MI or sham groups; experimental conditions were standardized to every degree possible, meaning end points of comprehensive hemodynamics (as descried below) were used and analysis was blinded when possible (i.e., for histological analysis and isolated lung perfusion analysis).

Echocardiography. Transthoracic echocardiography was conducted to assess left ventricular (LV) morphology and function in vivo. As previously described, mice were anesthetized with 5% isoflurane and then maintained with 1–2% isoflurane and room air throughout the procedure; body temperature was maintained at 37°C using a heated platform (16, 21). Echocardiographic parameters were measured over at least three consecutive cardiac cycles and averaged.

In vivo RV and pulmonary vascular hemodynamics. Surgical preparation, hemodynamic measurements, and analysis were based on established protocols (20, 21, 65, 70). Anesthesia was induced with an intraperitoneal injection of urethane solution (1 mg/g body weight) to maintain heart rate. Mice were then intubated and placed on a ventilator (Harvard Apparatus, Holliston, MA). As previously described, the thoracic cavity was entered, and the heart was exposed by removal of anterior rib cage (21, 65, 70). This open chest technique was used because the stiffness of the catheter used for RV pressure and volume measurements precludes a closed chest approach with catheter insertion through the jugular vein. LV pressure was measured with a pressure catheter (Millar, Houston, TX) inserted from the common carotid artery and advanced through the aortic valve into the LV. Heart rate and systemic pressure were recorded and observed throughout the procedure. RV pressure-volume loops were obtained as previously described using a 1.2-Fr admittance catheter inserted through the apex of the heart into the RV. After instrumentation was established and baseline pressure-volume measurements were obtained, the inferior vena cava was isolated and briefly occluded to obtain alterations in venous return for determination of end-systolic and end-diastolic pressure relations. One MI mouse expired shortly following placement of the catheter into the RV such that only pressure measurements could be obtained. A second MI mouse expired during inferior vena cava occlusions, and only baseline pressure-volume loops were obtained for that animal. Commercial software (Notocord; Croissy Sur Seine, France) recorded RV pressure and volume waveforms simultaneously, and data were analyzed using a minimum of 10 consecutive cardiac cycles. Cardiac output (CO) was normalized by body weight to calculate the cardiac index (20, 21, 36, 65, 70).

Pulmonary vascular mechanical function was quantified using total pulmonary vascular resistance (TPVR), PVR, and transpulmonary gradient (TPG). TPVR was calculated as mPAP divided by CO, where mPAP was assumed to be equal to right ventricular end-systolic pressure (RVSP) (7, 65). PVR was determined as (mPAP-mLAP/CO) where mLAP was assumed equal to LV end diastolic pressure (LVEDP) (5). TPG was computed as mPAP minus mLAP.

RV mechanical function was assessed using established parameters including maximum and minimum pressure derivatives (dP/dt_{max}, dP/dt_{min}), end-systolic elastance (E_{es}), and the slope of dP/dt_{max}-end diastolic volume (V_{ed}) relationship obtained from inferior vena cava occlusions (21, 57, 70). Ventricular-vascular interactions were assessed using E_{es}/arterial elastance (E_a) (21, 70). Finally, cardiac energetics were assessed via pressure-volume area (PVA), external mechanical work (EW), and ventricular mechanical efficiency (EW/PVA) as previously reported (45, 55).

Ex vivo pulmonary vascular pressure-flow dynamics. The isolated, ventilated, perfused lung preparation was used as previously validated and detailed by our group (73, 76). Briefly, following euthanasia with 150 mg/kg of pentobarbital, the trachea was cannulated for ventilation. The lungs were ventilated with room air between end expiratory and end inspiratory pressures of ~1 and ~8 mmHg, respectively.

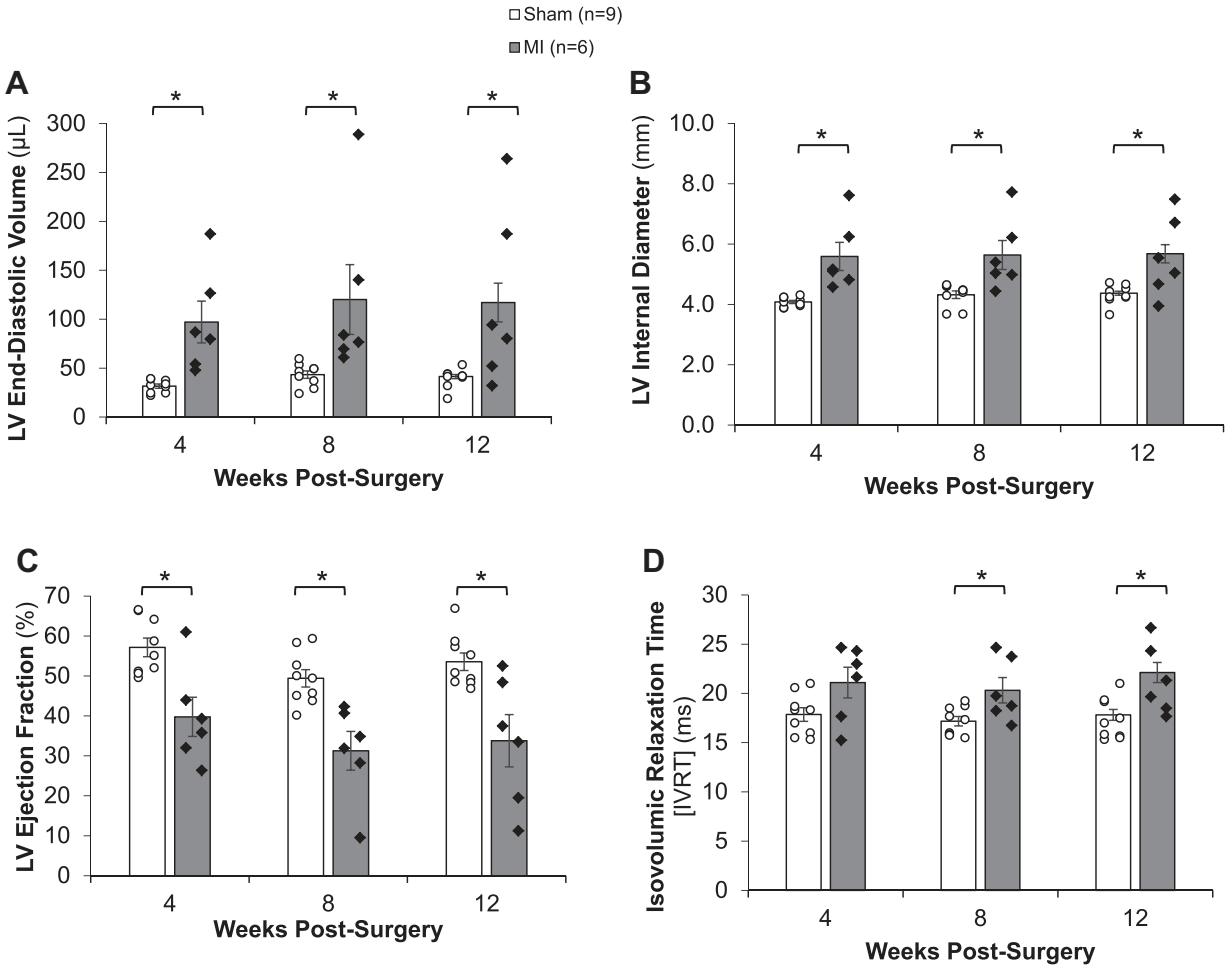

Fig. 1. Development of left ventricular (LV) dysfunction and dilation post-myocardial infarction (MI). *A–D*: increased LV size develop by 4 wk post-MI and persist through 12 wk (*A* and *B*) and are associated with impaired systolic function measured by reduced LV ejection fraction (*C*) and impaired diastolic function measured by increased isovolumic relaxation time (IVRT; *D*). *$P < 0.05$ vs. sham.

Following cannulation of the trachea, 1 ml of heparin (1.25 mg/ml) was injected into the RV to prevent clots from forming in the pulmonary vasculature (76). Subsequently, the pulmonary artery (PA) and left atrium were cannulated for perfusate inflow and outflow, respectively (76, 77). The lungs were perfused with warm RPMI 1640 cell culture medium with 3.5% Ficoll (an oncotic agent). Steady-state perfusion was conducted using a syringe pump and pulsatile flow was achieved using a high-frequency oscillatory pump in parallel with the syringe pump. Pressure transducers (ADT300; Harvard Apparatus, Holliston, MA) were used to measure PAP, left atrium pressure (LAP), as well as airway pressure (MPX; Harvard Apparatus, Holliston, MA). Perfusate inflow (Q) was monitored using an in-line flow meter (MEI PXN; Transonic Systems, Ithaca, NY). Pressures and flows were continuously monitored on a computer display and were recorded at 200 Hz (77). Lungs were monitored for development of edema. One set of sham lungs developed edema, and the experiment was stopped before collection of pulsatile perfusion data.

The pulsatile flow measurements were performed and recorded as previously validated (73, 76). The lungs were initially perfused with RPMI at 1 ml/min for 2 min or until lungs were fully perfused and had turned white. The flow rate was then increased to 3 ml/min, and sinusoidal flow rates of the form $Q = 3 + 2 \sin(2\pi ft)$ ml/min were generated for frequencies of $f = 1, 2, 5, 10, 15$, and 20 Hz. This range of frequencies was chosen to fully include the physiologic heart rate of mice (~10 Hz) (73). The lungs were held at end expiratory pressure (~1 mmHg) throughout data collection, and PAP, LAP, and Q were recorded as described above. Immediately following the pulsatile flow protocol, the lungs were allowed to rest at a flow rate of 0.5mL/min for 1 min and normal ventilation was resumed, along with intermittent deep inspirations of ~15 mmHg to maintain airway patency.

After the pulsatile flow protocol and rest period, steady-state measurements were obtained. First, the flow rate was increased to 1 ml/min and then flow rate was increased to 5 ml/min in increments of 1 ml/min with PAP, LAP, and Q recorded once steady state was

Table 1. *Biventricular morphometric changes due to MI*

Tissue	Sham	MI	*P* Value
n	14	12	
BW, g	29.5 ± 0.63	29.3 ± 0.48	0.969
LA/BW	0.12 ± 0.01	0.21 ± 0.01	**0.002**
LV + S, mg	92.4 ± 2.9	128.3 ± 7.8	**<0.001**
LV + S/BW, mg	3.1 ± 0.07	4.4 ± 0.24	**<0.001**
RA/BW	0.14 ± 0.01	0.16 ± 0.02	0.368
RV, mg	23.3 ± 0.9	30.5 ± 1.7	**<0.001**
RV/BW, mg/g	0.79 ± 0.03	1.04 ± 0.08	**<0.001**
RV/LV + S, mg/mg	0.25 ± 0.01	0.24 ± 0.01	0.338
Lungs/BW*	4.5 ± 0.1	4.9 ± 0.3	0.267

Values are means ± SE. BW, body weight; LV + S, left ventricle and septum; RV, right ventricle; LA, left atrium; R, right atrium; MI, myocardial infarction. Bold indicates significance. *$n = 6$ for sham, $n = 9$ for MI.

Table 2. *In vivo metrics of right ventricle and pulmonary vasculature function*

Parameter	Sham	MI	*P* Value
n	9	6	
Heart rate, beats/min	554 ± 12	521 ± 24	0.231
LV end-systolic pressure, mmHg	76 ± 7.0	66 ± 6.5	0.096
LV end-diastolic pressure, mmHg	2.0 ± 0.1	8.6 ± 1.5	**0.010**
Right ventricular indexes			
RV systolic pressure, mmHg	19.6 ± 1.0	29.0 ± 1.2	**<0.001**
RV diastolic pressure, mmHg	0.74 ± 0.69	4.42 ± 1.44	**0.029**
End-systolic volume, μl	18.2 ± 1.6	13.4 ± 1.7	0.102
End-diastolic volume, μl	37.3 ± 3.5	26.7 ± 2.0	0.055
Cardiac output, ml/min	10.6 ± 1.1	7.0 ± 0.8	**0.048**
Systolic indexes			
RV ejection fraction, %	50.5 ± 2.7	49.8 ± 3.9	0.881
dP/dt_{max}, mmHg/s	1590 ± 160	1633 ± 150	0.848
dP/dt_{max} end-diastolic volume, $mmHg \cdot s^{-1} \cdot \mu l$	49.1 ± 8.4	61.4 ± 6.7	0.292
Stroke work, mmHg/μl	357 ± 41	365 ± 110	0.919
Diastolic indexes			
dP/dt_{min}, mmHg/s	−1,230 ± 160	−1,200 ± 140	0.894
Relaxation factor τ, ms	8.9 ± 1.9	16.2 ± 3.0	**0.049**
Chamber compliance, μl/mmHg	1.00 ± 0.14	0.54 ± 0.06	**0.044**
Pulmonary vascular indexes			
Total pulmonary vascular resistance, $mmHg \cdot min^{-1} \cdot ml$	2.05 ± 0.29	4.49 ± 0.73	**0.004**
Pulmonary vascular resistance, $mmHg \cdot min^{-1} \cdot ml$	1.61 ± 0.21	3.70 ± 0.40	**0.026**
Transpulmonary pressure gradient, mmHg	16.6 ± 1.1	21.7 ± 1.0	**0.045**

Values are means ± SE. LV, left ventricular; RV, right ventricular. MI, myocardial infarction. Bold indicates significance.

reached. The flow rate was then decreased from 5 to 1 ml/min, again at 1 ml/min increments as soon as steady state was reached. The lungs were held at end expiratory pressure (~1 mmHg) throughout data collection.

From the steady state flow protocol, TPG was calculated as PAP − LAP and PVR was calculated as TPG/Q for each flow rate. Distensibility, α, was determined from the steady-state pressure-flow curve as previously described (43, 64). Pulmonary vascular impedance magnitude (*Z*) and phase (θ) were calculated from one full sinusoidal cycle of ΔP = PAP – LAP and Q at each frequency tested (77). Input resistance Z_0 was calculated from the average impedance at the 0th harmonic of all frequencies. Characteristic impedance Z_C was calculated as the average impedance between the first minimum (5 Hz) and highest frequency imposed (20 Hz) (77). Wave reflection R_w was calculated as $(Z_0 - Z_c)/(Z_0 + Z_c)$ (76).

Tissue harvest, fixation, and histology. Following either completion of the isolated lung procedure or right heart catheterization, the heart and lungs were removed from the mouse. The RV was then separated from the LV and septum, and the LA and RA were also separated. Heart tissues were weighed and then divided for preservation by either flash freezing or placement in 10% formalin. The right and left lungs were separated and weighed. The right lung was preserved in 10% formalin, and the left lung was flash frozen.

Harvested tissues following right heart catheterization that were fixed in 10% formalin as described above were preserved in 70% ethanol. Tissues were then embedded in paraffin, sectioned, and stained as detailed below for histological analysis.

Perivascular pulmonary fibrosis. Pulmonary sections were stained with picrosirius red to assess collagen deposition, as previously described (21, 79). An inverted microscope (TE-2000-5; Nikon, Melville, NY) was used to acquire histological images using a Spot CCD camera (Optical Analysis Systems, Nashua, NH). The area of perivascular collagen was determined using color thresholding in a representative field of view by an observer blinded to the experimental groups using MetaVue software (Optical Analysis Systems). In the RV, collagen area was divided by total tissue area of the representative image to calculate collagen area percent (21, 79). In pulmonary arterioles, collagen area was divided by the perimeter of the identified arteriole. Pulmonary arterioles were differentiated from venules by their immediate proximity to airways (72). Arteriole diameters ranged from 50 to 200 μm.

Pulmonary vascular remodeling. Verhoeff-Van Giesson immunohistochemical staining was performed on paraffin-embedded lung sections as previously described (22). In a blinded fashion, pulmonary arteries <200 μm in diameter were identified by proximity to terminal bronchioles or alveolar ducts under a ×20 objective as previously described (41). Images were obtained using an Olympus BX41 microscope with Olympus camera. At least 20 vessels per animal were sampled, and the wall fraction [(total area – luminal area)/total area)] was calculated using ImageJ software.

RV capillarization. RV sections were stained with DAPI (staining nuclei; Prolong Gold with Dapi antifade mounting media; Life Technologies-ThermoFisher) and antibodies directed against lectin *Griffonia simplicifolia* (staining capillary endothelial cells; 1:75; Life Technologies- ThermoFisher) or wheat germ agglutinin (1:

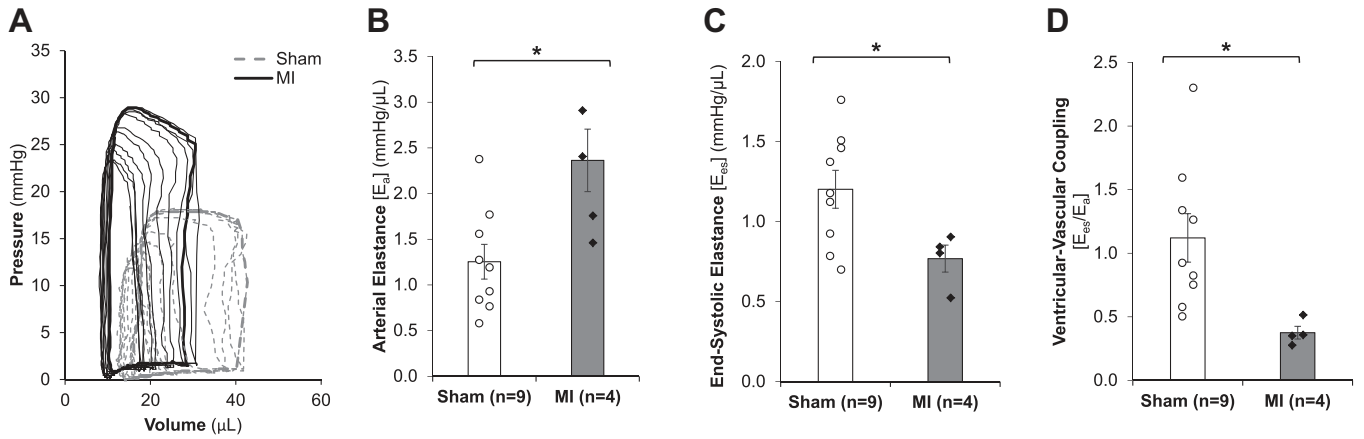

Fig. 2. Right ventricular-pulmonary vascular uncoupling following myocardial infarction (MI). *A*: representative pressure-volume loops in sham and MI mouse right ventricles. Data obtained during alteration of preload by occlusion of the inferior vena cava occlusions. *B–D*: increased arterial elastance (E_a; *B*) and decreased end-systolic elastance (E_{es}; *C*) result in impaired ventricular-vascular coupling (E_{es}/E_a; *D*) at 12 wk post-MI. *$P < 0.05$ vs. sham.

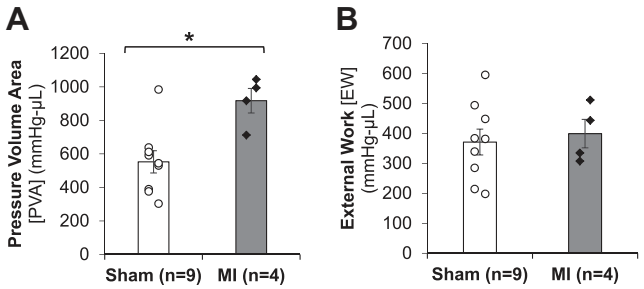

Fig. 3. Myocardial infarction (MI) leads to increased right ventricular (RV) oxygen consumption and decreased mechanical efficiency. *A–C*: increased oxygen consumption measured by pressure-volume area (PVA; *A*) with no change in RV external work (EW; *B*) result in reduced mechanical efficiency (EV/PVA; *C*) at 12 wk post-MI.*$P < 0.05$ vs. sham.

500; Life Technologies-ThermoFisher). Capillaries were identified by lectin positivity and cardiomyocytes were identified by wheat germ agglutinin staining (27). The number of capillaries and cardiomyocytes per field was counted by a blinded investigator, and capillary density was then expressed as capillary/cardiomyocyte ratio (22, 27). Five fields with cross sectionally cut cardiomyocytes were analyzed per animal.

Western blotting. Western blotting was performed by a blinded investigator on whole lung homogenates as previously described (15). Briefly, lung tissue was homogenized with an Omni international tissue grinder (Thermo Fisher Scientific, Waltham, MA) in ice-cold RIPA lysis buffer (Pierce-Thermo Fisher Scientific) containing proteinase inhibitor cocktail (EMD-Millipore-Sigma Aldrich, St. Louis, MO) and PhosStop inhibitor cocktail (Roche, Pleasanton, CA). After homogenization, the lysate was sonicated (for ten 1-s pulses at 100% power) and then centrifuged. The supernatant was saved and used as whole lung lysate. Protein concentration was measured using BCA Protein Assay (Pierce-ThermoFisher Scientific). Antibodies used were proliferating cell nuclear antigen (PCNA; 1:500; Abcam, Cambridge, MA) and vinculin (1:5,000; Calbiochem; Billerica, MA). Densitometry was performed via ImageJ.

Statistical Analysis. All values are presented as means ± SE. Student's *t*-test was used to compare between sham and MI groups. Repeated measures ANOVA was used to compare serial measurements within groups. Bivariate correlations were performed using Pearson's correlation analysis. All *P* values were two-sided, and $P < 0.05$ was taken as statistically significant.

RESULTS

Impaired LV function post-MI. Cardiac function was evaluated by echocardiography following MI. Echocardiographic imaging demonstrated evidence of LV dilation with a near doubling of LVEDV and nearly 30% increased LV internal diameter occurring by 4 wk post-MI (Fig. 1, *A* and *B*). These increases in LVEVD and LV internal diameter were sustained through 12 wk post-MI. As a consequence, there was significant impairment in LV systolic function, as evidence by a 30% decrease in LV ejection fraction (EF) as soon as 4 wk post-MI (Fig. 1*C*). This decrease in EF persisted through 12 wk post-MI without evidence of recovery. There was evidence of diastolic dysfunction as measured by increased isovolumetric relaxation time at 8 and 12 wk post-MI (Fig. 1*D*). These impairments in systolic and diastolic function as well as LV dilation are consistent with the development of left heart failure post-MI.

Biventricular remodeling post-MI. Tissue analysis at 12 wk post-MI demonstrated biventricular remodeling. Both left atrial weight and LV weight, which includes LV + septum, were elevated, demonstrating left sided cardiac remodeling (Table 1), which is consistent with the LV dilation determined by echocardiography (Fig. 1, *A* and *B*). Additionally, there was a significant increase in the absolute RV weight as well as the RV weight indexed to body weight. Interestingly, the Fulton index (RV weight indexed to the weight of LV + septum) was unchanged, indicating RV hypertrophy occurred in proportion to LV remodeling (Table 1). Analysis of lung tissues demonstrated a trend toward increased wet lung weight that did not reach statistical significance.

Development of secondary PH and RV dysfunction post-MI. Invasive hemodynamic measurements were obtained at 12 wk post-MI. LVEDP increased over fourfold following MI (Table 2). In addition, there was a significant increase in RVSP (Table 2), demonstrating the development of secondary PH. Consistent with this, there was a doubling of the TPVR and a significant increase in the TPG in the post-MI group. There was also a significant elevation in RV afterload as measured by the E_a (Fig. 2, *A* and *B*). Hemodynamic analysis further demonstrated significantly lower CO post-MI (Table 2), which is consistent with the development of heart failure with reduced ejection fraction (HFrEF).

In the setting of reduced CO, RV systolic function was largely preserved as demonstrated by maintained RV EF and stroke work (Table 2). Despite maintained function by some indexes, pressure-volume loops obtained with varying preload

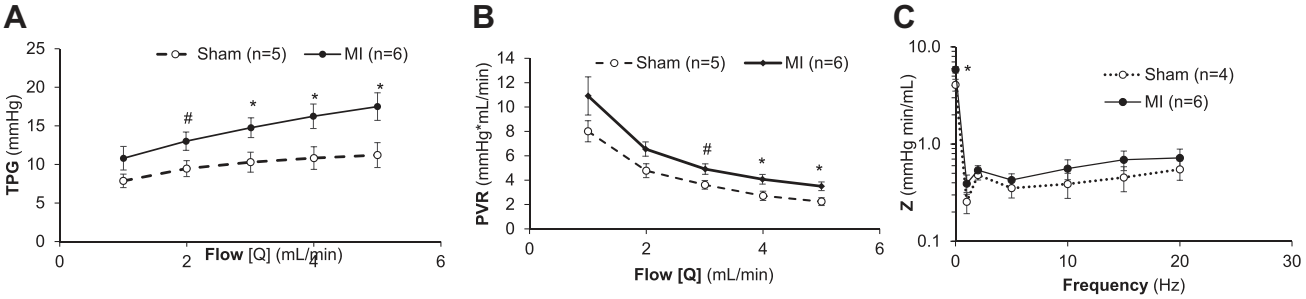

Fig. 4. Increased pulmonary vascular resistance and impedance following myocardial infarction (MI). *A* and *B*: steady isolated lung perfusion demonstrated elevated trans pulmonary gradient (TPG; *A*) and increased pulmonary vascular resistance (PVR; *B*). *C*: pulsatile perfusion demonstrated increased impedance (*Z*) at 0 Hz. *$P < 0.05$ vs. sham. #$P = 0.05$ vs. sham.

Table 3. *Ex vivo metrics of pulmonary vascular function*

Tissue	Sham	MI	*P* Value
n	5	6	
Input resistance, Z_0, mmHg·min^{-1}·ml	4.01 ± 0.57	5.83 ± 0.44	**<0.05**
Characteristic impedance, Z_c, mmHg·min^{-1}·ml	0.44 ± 0.11	0.60 ± 0.12	0.375
Wave reflection index, R_w	0.81 ± 0.02	0.82 ± 0.03	0.941
Distensibility, α, 1/mmHg	0.037 ± 0.005	0.027 ± 0.004	0.176

Values are means ± SE. MI, myocardial infarction. Bold indicates significance.

(Fig. 2*A*) demonstrate a significant decrease in E_{es} (Fig. 2, *A* and *C*). In combination with the increased RV afterload (E_a), decreased E_{es} resulted in RV-pulmonary vascular uncoupling (Fig. 2*D*). In the setting of PAH, ventricular-vascular uncoupling suggests development of RV dysfunction and is predictive of increased mortality (1, 6, 32, 38, 58). In addition, increased τ and decreased chamber compliance provide evidence of RV diastolic dysfunction (Table 2). There was a trend toward decreased RV volumes as measured by right heart catheterization (Table 2). These findings were consistent with echocardiographic assessments that demonstrated no change in RV internal diameter (data not shown).

We further evaluated RV mechanical energy consumption and output. There was a significant increase in RV energy consumption, as measured by PVA (Fig. 3*A*). However, despite this increase in consumption, RV mechanical energy output as measured by EW was similar to sham (Fig. 3*B*). Taken together, this resulted in a significant decrease in EW/PVA occurring in the setting of post-MI secondary PH (Fig. 3*C*).

Increased PVR and impedance post-MI. In vivo hemodynamic analysis demonstrated increased afterload measured by E_a (Fig. 2*B*) in addition to increased TPVR and LVEDP (Table 2), indicating the development of PH-LHF. In addition, there was significant elevation in the TPG. To better characterize maladaptive changes in the pulmonary vasculature, we performed ex vivo isolated lung perfusion at 12 wk post-MI. Figure 4*A* demonstrates increased TPG at flow rates between 2 and 5 ml/min in post-MI lungs. Consistent with increased TPG, PVR was significantly elevated in the post-MI lungs at flow rates from 3 to 5 ml/min (Fig. 4*B*), indicating a progression to Cpc-PH potentially driven by vasoconstriction or remodeling of the pulmonary vasculature in the post-MI setting. Pulmonary vascular impedance was evaluated using a pulsatile flow protocol as described above. The input resistance, Z_0, was significantly elevated in the post-MI group (Fig. 4*C* and Table 3). There was a trend toward increased Z_c, a measure of proximal artery stiffness, which did not reach statistical significance, and no change in wave reflection index, R_w, an indicator of pulse pressure wave reflections (Table 3). Similar to the findings for Z_c, there was a trend toward reduced distensibility, α, which was not statistically significant (Table 3).

Development of perivascular pulmonary fibrosis without medial hypertrophy or increased proliferation post-MI. Histological examination of the pulmonary vasculature was completed to determine if the observed changes in pulmonary vascular function (increased PVR, E_a, and Z_0) were associated

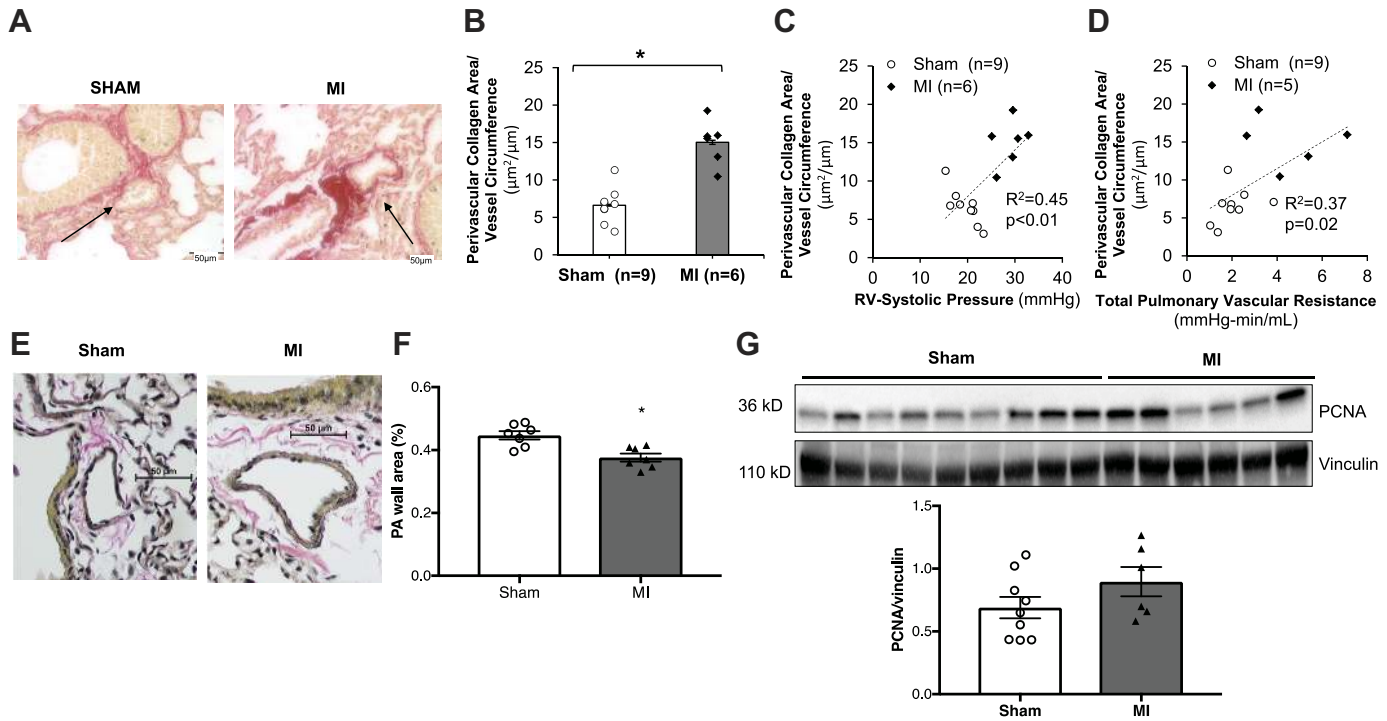

Fig. 5. Development of perivascular pulmonary fibrosis following myocardial infarction (MI). *A* and *B*: picrosirus red staining demonstrates increased perivascular collagen deposition in pulmonary arteries (PAs) (marked by arrows) post-MI. *C* and *D*: amount of perivascular collagen correlates with right ventricle (RV)-systolic pressure (*C*) and total pulmonary vascular resistance (TPVR) (*D*). *$P < 0.05$ vs. sham. *E* and *F*: remodeling was assessed by Verhoeff-van Giesson staining (*E*) and calculation of PA wall area fraction (PA wall area/total vessel area; *F*) in PAs <200 μm. Representative images are shown. Size bars = 50 μm. *$P < 0.05$ by *t*-test. *G*: proliferating cell nuclear antigen (PCNA) was measured in lung homogenates from sham or MI animals by Western blotting and densitometric quantification. Vinculin was used as loading control.

with structural changes. Picrosirus red staining demonstrated significant increase in perivascular collagen deposition in pulmonary arterioles (Fig. 5, *A* and *B*). The amount of perivascular collagen correlated with both RVSP, a surrogate for mPAP, and TPVR (Fig. 5, *C* and *D*). These findings demonstrate that perivascular remodeling characterized by increased collagen deposition is one mechanism contributing to the development of increased PVR in secondary PH. Pulmonary arterial remodeling was further assessed by examination of medial hypertrophy using Verhoeff-van Giesson staining and calculation of PA wall area fraction (Fig. 5, *E* and *F*). Analysis demonstrated no evidence of medial hypertrophy in the post-MI group, which actually showed a slight decrease in PA wall area fraction compared with control. To assess for PA cell proliferation, PCNA expression was measured in lung homogenates from sham or MI animals. As demonstrated in Fig. 5*G* there was no difference in PCNA between the sham and MI groups.

Absence of RV fibrosis or change in capillarity density post-MI. Histological examination of the RV was also performed. As shown in Fig. 6, there were no changes in collagen content or RV capillary density.

DISCUSSION

This study investigated the mechanical mechanisms of pulmonary vascular and RV dysfunction due to secondary PH in a mouse model of ischemic HFrEF. We observed the following changes in the pulmonary vasculature: increased PVR, Z_0, and E_a. These were associated with perivascular fibrosis in the pulmonary arteries. RV diastolic dysfunction occurred in addition to reduced E_{es} and ventricular-vascular uncoupling. While cardiac output decreased in the setting of MI leading to HFrEF, RV EF was preserved, indicating that RV failure had not yet developed.

Our findings of increased LVEDP, RVSP, and RV hypertrophy are consistent with previous studies showing evidence of PH-LHF in rodent models (2, 8, 31, 33, 37, 49, 56, 61, 80). In addition to documenting the development of PH in a murine model of HFrEF, this study demonstrated changes in the pulmonary vascular response to steady and pulsatile flow developing in this context through both in vivo and ex vivo assessments. This comprehensive approach enabled demonstration of progression to Cpc-PH from Ipc-PH post-MI. Moreover, from ex vivo pulmonary vascular pressure-flow dynamics, we demonstrated that Cpc-PH in this model is not characterized by a change in characteristic impedance (indicative of proximal arterial stiffening) in contrast to findings in small animal models of PAH (44, 74). Interestingly, there was also no change in distensibility of the small pulmonary arterioles. A recent study demonstrated that reduced pulmonary vascular distensibility was correlated with degree of PH, exercise capacity, and survival in patients with PH-LHD (47). This patient cohort had significant reduction in RV EF indicating severe disease with RV EF. However, at 12 wk postsurgery in the MI mice, the PH was moderate and RV EF was maintained. Thus significant changes in pulmonary arteriolar distensibility may require more severe disease or longer term PH.

Structural changes underlying the increased resistance and impedance were identified in the pulmonary vasculature. There was a significant increase in perivascular collagen in the pulmonary arteries, which is consistent with previous reports of pulmonary fibrosis in a rodent models of PH-LHF (8, 33) as well as with pulmonary vascular remodeling consistently found in

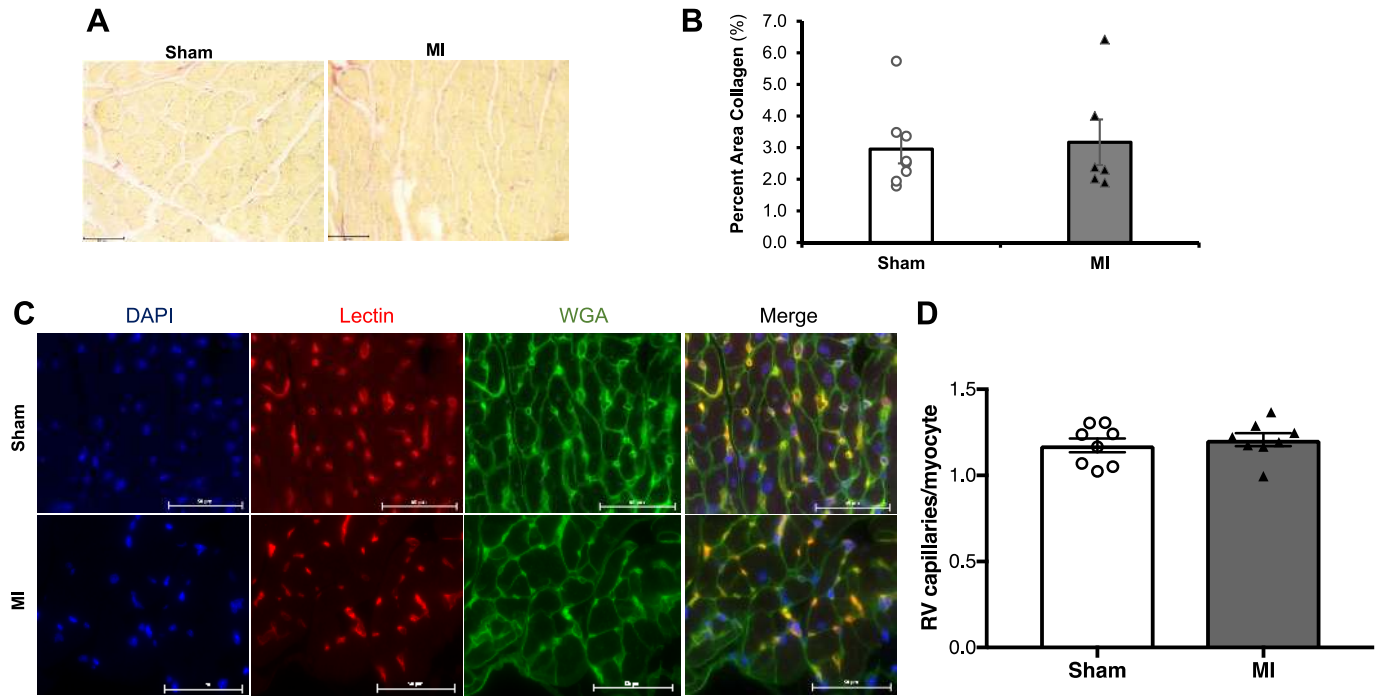

Fig. 6. No right ventricular (RV) remodeling seen following myocardial infarction (MI). *A* and *B*: Picrosirus red staining shows low levels of RV collagen in MI and sham mice. Scale bars = 50 μm. *C* and *D*: RV capillarization was determined in RV sections by staining nuclei (DAPI; blue), endothelial cells (lectin Griffonia simplicifolia; red) and cell membranes [wheat germ agglutinin (WGA); green]. Capillaries were identified by lectin positivity; cardiomyocytes were identified by WGA staining. The number of capillaries per field was then normalized to the number of myocytes (expressed as capillary/myocyte ratio). Representative images are shown. Scale bars = 50 μm.

small animal models of PAH (67–69). Additionally, the presence of structural remodeling of the pulmonary vasculature has been demonstrated on autopsy specimens of patients with Cpc-PH who died following heart transplant (11). The current study goes beyond previous investigations of PH-LHF in demonstrating functional mechanical changes associated with these histological changes. This study demonstrates mechanical changes in the pulmonary vasculature including increased PVR without evidence of changes in proximal PA stiffness (i.e., no change in characteristic impedance). Consistent with these findings, there is evidence of perivascular pulmonary arterial fibrosis without evidence of medial hypertrophy or increased proliferation, two traditional hallmarks of pulmonary vascular remodeling in PAH (30, 34, 48). Thus this model likely represents an early stage of Cpc-PH in which some of the precapillary component of the PH is due to vasoconstriction and potentially reversible. These results highlight that the types and mechanisms of pulmonary vascular remodeling in PH-LHF are potentially different than those well characterized in PAH. Further studies are needed to quantify the pulmonary venous and capillary remodeling, which likely occur before pulmonary arterial remodeling in PH-LHF and were unable to be fully assessed in the current study.

Beyond evaluation of the pulmonary vasculature, RV mechanical function was evaluated through in vivo pressure-volume loop analysis. We demonstrate the development of RV dysfunction with reduced E_{es} and impaired ventricular-vascular coupling as well as impaired diastolic function (decreased compliance and increased τ). A recent study in human patients with PH-LHF showed reduced RV pulmonary vascular coupling in Cpc-PH compared with Ipc-PH (17). RV diastolic dysfunction has been demonstrated in patients with LHF; interestingly, RV diastolic dysfunction did not correlate with degree of PH and occurred in patients with LHF without PH (81). There was no RV dilation found in our PH-LHF model, which is consistent with a state of RV dysfunction rather than failure as RV dilation has been shown to occur late in the progression to RV failure (3, 78).

While this study provides important insights into PH-LHF, there are important limitations to note. Invasive measurements of pulmonary vascular and RV function were completed at a single time point. Therefore, causal relationships between RV and pulmonary vascular hemodynamic changes or between structural and functional changes cannot be determined. We document RV hypertrophy but did not elucidate when it occurs in relationship to LV remodeling and increased PVR. The post-MI mice show evidence of Cpc-PH, but we cannot differentiate the contributions of reversible vasoconstriction from irreversible remodeling (unresponsive to vasodilators) to the Cpc-PH. The presence of pulmonary vascular fibrosis suggests progression to a fixed disease state; however, other markers of pulmonary arterial remodeling were negative. The response to pulmonary vasodilators would enable the active versus passive mechanical mechanisms of Cpc-PH to be distinguished. Additionally, further evaluation of pulmonary vascular remodeling including PA calcification, pulmonary capillary remodeling, and pulmonary venous remodeling are important areas to be addressed in future work. It is important to note that diastolic pressure gradient, the primary metric for distinguishing Ipc-PH and Cpc-PH in clinical practice, was not able to be determined as PAPs were not directly measured in vivo. Both PVR and TPG, two key features of Cpc-PH (28, 50), were assessed both in vivo and ex vivo. In particular, ex vivo isolated, ventilated, lung perfusion where measurements are taken across varying flow rates overcome many of the limitations of in vivo assessments, the primary of which is that they are flow dependent (52, 53). Furthermore, all in vivo pressure measurements were acquired using an open-chest technique and intravenous anesthesia (urethane) was used, which can cause artifactual reductions in pressures (62). It is likely but unknown whether these factors would impact both groups similarly and thus are key limitations that must be taken into account in interpreting the results. Despite these limitations, this work uncovers mechanical mechanisms in the pulmonary vascular and RV progression of disease in a rodent model of HFrEF.

Conclusion. This study is among the few to quantify pulmonary vascular biomechanics in a small animal model of HFrEF leading to PH-LHF. It goes beyond previous reports in models of PH-LHF to provide a both robust and comprehensive evaluation of pulmonary vascular and RV mechanical function. Cpc-PH associated with increased PVR, input resistance, and arterial E_a is shown to develop by 12 wk post-MI in mice. These hemodynamic changes correlate with structural remodeling in the pulmonary vasculature. We further quantified RV mechanical function in the setting of Cpc-PH due to HFrEF and demonstrate diastolic dysfunction and ventricular-vascular uncoupling consistent with findings in patients with PH-LHF. Future studies are needed to evaluate the time course and progression of pulmonary vascular and RV mechanical changes in PH-LHF as well as the molecular drivers of these mechanical mechanisms.

ACKNOWLEDGMENTS

We thank Gaoussou Diarra and Allison Rogers for technical support.

GRANTS

This work was supported, in part, by a Thoracic Surgery Foundation Nina Starr Braunwald Research Fellowship (to J. L. Philip); National Heart, Lung, and Blood Institute Grant R01-HL-086939 (to N. C. Chesler); American Heart Association Grant AHA-17POST33670365 (to A. L. Frump); and Veterans Affairs Merit Grant 1I01BX002042-05 (to T. Lahm).

DISCLOSURES

T. Lahm serves on the speaker bureau for Bayer, has served as a consultant for Actelion and Gilead, and has received research reagents from Eli Lilly & Co. No other conflicts of interest, financial or otherwise, are declared by the authors.

AUTHOR CONTRIBUTIONS

J.L.P., D.M.T., A.L.F., T.A.H., T.L., and N.C.C. conceived and designed research; J.L.P., T.M.M., D.A.S., S.S., M.A., and T.A.H. performed experiments; J.L.P., T.M.M., S.S., M.A., and N.C.C. analyzed data; J.L.P., T.M.M., D.A.S., D.M.T., A.L.F., T.A.H., T.L., and N.C.C. interpreted results of experiments; J.L.P., T.M.M., A.L.F., and T.L. prepared figures; J.L.P. drafted manuscript; J.L.P., D.M.T., T.A.H., T.L., and N.C.C. edited and revised manuscript; J.L.P., T.M.M., D.A.S., T.L., and N.C.C. approved final version of manuscript.

REFERENCES

1. **Alaa M, Abdellatif M, Tavares-Silva M, Oliveira-Pinto J, Lopes L, Leite S, Leite-Moreira AF, Lourenço AP.** Right ventricular end-diastolic stiffness heralds right ventricular failure in monocrotaline-induced pulmonary hypertension. *Am J Physiol Heart Circ Physiol* 311: H1004–H1013, 2016. doi:10.1152/ajpheart.00202.2016.
2. **Ben Driss A, Devaux C, Henrion D, Duriez M, Thuillez C, Levy BI, Michel JB.** Hemodynamic stresses induce endothelial dysfunction and

remodeling of pulmonary artery in experimental compensated heart failure. *Circulation* 101: 2764–2770, 2000. doi:10.1161/01.CIR.101.23.2764.

3. **Bogaard HJ, Abe K, Vonk Noordegraaf A, Voelkel NF.** The right ventricle under pressure: cellular and molecular mechanisms of right-heart failure in pulmonary hypertension. *Chest* 135: 794–804, 2009. doi:10.1378/chest.08-0492.
4. **Bonnet S, Provencher S, Guignabert C, Perros F, Boucherat O, Schermuly RT, Hassoun PM, Rabinovitch M, Nicolls MR, Humbert M.** Translating research into improved patient care in pulmonary arterial hypertension. *Am J Respir Crit Care Med* 195: 583–595, 2017. doi:10.1164/rccm.201607-1515PP.
5. **Braunwald E, Frahm CJ.** Studies on Starling's Law of the Heart. IV. Observations on the hemodynamic functions of the left atrium in man. *Circulation* 24: 633–642, 1961. doi:10.1161/01.CIR.24.3.633.
6. **Brewis MJ, Bellofiore A, Vanderpool RR, Chesler NC, Johnson MK, Naeije R, Peacock AJ.** Imaging right ventricular function to predict outcome in pulmonary arterial hypertension. *Int J Cardiol* 218: 206–211, 2016. doi:10.1016/j.ijcard.2016.05.015.
7. **Chemla D, Hébert JL, Coirault C, Salmeron S, Zamani K, Lecarpentier Y.** Matching dicrotic notch and mean pulmonary artery pressures: implications for effective arterial elastance. *Am J Physiol* 271: H1287–H1295, 1996. doi:10.1152/ajpheart.1996.271.4.H1287.
8. **Chen Y, Guo H, Xu D, Xu X, Wang H, Hu X, Lu Z, Kwak D, Xu Y, Gunther R, Huo Y, Weir EK.** Left ventricular failure produces profound lung remodeling and pulmonary hypertension in mice: heart failure causes severe lung disease. *Hypertension* 59: 1170–1178, 2012. doi:10.1161/HYPERTENSIONAHA.111.186072.
9. **Chesler NC, Roldan A, Vanderpool RR, Naeije R.** *How to measure pulmonary vascular and right ventricular function*. Annual International Conference of the IEEE Engineering in Medicine and Biology Society IEEE Engineering in Medicine and Biology Society Annual Conference 2009. Minneapolis, MN, 2009, p. 177–180.
10. **de Groote P, Millaire A, Foucher-Hossein C, Nugue O, Marchandise X, Ducloux G, Lablanche JM.** Right ventricular ejection fraction is an independent predictor of survival in patients with moderate heart failure. *J Am Coll Cardiol* 32: 948–954, 1998. doi:10.1016/S0735-1097(98)00337-4.
11. **Delgado JF.** The right heart and pulmonary circulation (III). The pulmonary circulation in heart failure. *Rev Esp Cardiol* 63: 334–345, 2010. doi:10.1016/S0300-8932(10)70092-0.
12. **Delgado JF, Conde E, Sánchez V, López-Ríos F, Gómez-Sánchez MA, Escribano P, Sotelo T, Gómez de la Cámara A, Cortina J, de la Calzada CS.** Pulmonary vascular remodeling in pulmonary hypertension due to chronic heart failure. *Eur J Heart Fail* 7: 1011–1016, 2005. doi:10.1016/j.ejheart.2004.10.021.
13. **Di Salvo TG, Mathier M, Semigran MJ, Dec GW.** Preserved right ventricular ejection fraction predicts exercise capacity and survival in advanced heart failure. *J Am Coll Cardiol* 25: 1143–1153, 1995. doi:10.1016/0735-1097(94)00511-N.
14. **Fang JC, DeMarco T, Givertz MM, Borlaug BA, Lewis GD, Rame JE, Gomberg-Maitland M, Murali S, Frantz RP, McGlothlin D, Horn EM, Benza RL.** World Health Organization Pulmonary Hypertension group 2: pulmonary hypertension due to left heart disease in the adult–a summary statement from the Pulmonary Hypertension Council of the International Society for Heart and Lung Transplantation. *J Heart Lung Transplant* 31: 913–933, 2012. doi:10.1016/j.healun.2012.06.002.
15. **Frump AL, Selej M, Wood JA, Albrecht M, Yakubov B, Petrache I, Lahm T.** Hypoxia upregulates estrogen receptor β in pulmonary artery endothelial cells in a HIF-1α-dependent manner. *Am J Respir Cell Mol Biol* 59: 114–126, 2018. doi:10.1165/rcmb.2017-0167OC.
16. **Gao S, Ho D, Vatner DE, Vatner SF.** Echocardiography in Mice. *Curr Protoc Mouse Biol* 1: 71–83, 2011. doi:10.1002/9780470942390.mo100130.
17. **Gerges M, Gerges C, Pistritto AM, Lang MB, Trip P, Jakowitsch J, Binder T, Lang IM.** Pulmonary hypertension in heart failure. epidemiology, right ventricular function, and survival. *Am J Respir Crit Care Med* 192: 1234–1246, 2015. doi:10.1164/rccm.201503-0529OC.
18. **Ghio S, Gavazzi A, Campana C, Inserra C, Klersy C, Sebastiani R, Arbustini E, Recusani F, Tavazzi L.** Independent and additive prognostic value of right ventricular systolic function and pulmonary artery pressure in patients with chronic heart failure. *J Am Coll Cardiol* 37: 183–188, 2001. doi:10.1016/S0735-1097(00)01102-5.
20. **Golob MJ, Tian L, Wang Z, Zimmerman TA, Caneba CA, Hacker TA, Song G, Chesler NC.** Mitochondria DNA mutations cause sex-dependent development of hypertension and alterations in cardiovascular function. *J Biomech* 48: 405–412, 2015. doi:10.1016/j.jbiomech.2014.12.044.
21. **Golob MJ, Wang Z, Prostrollo AJ, Hacker TA, Chesler NC.** Limiting collagen turnover via collagenase-resistance attenuates right ventricular dysfunction and fibrosis in pulmonary arterial hypertension. *Physiol Rep* 4: e12815, 2016. doi:10.14814/phy2.12815.
22. **Goss KN, Cucci AR, Fisher AJ, Albrecht M, Frump A, Tursunova R, Gao Y, Brown MB, Petrache I, Tepper RS, Ahlfeld SK, Lahm T.** Neonatal hyperoxic lung injury favorably alters adult right ventricular remodeling response to chronic hypoxia exposure. *Am J Physiol Lung Cell Mol Physiol* 308: L797–L806, 2015. doi:10.1152/ajplung.00276.2014.
23. **Grant BJ, Lieber BB.** Clinical significance of pulmonary arterial input impedance. *Eur Respir J* 9: 2196–2199, 1996. doi:10.1183/09031936.96.09112196.
24. **Guazzi M, Borlaug BA.** Pulmonary hypertension due to left heart disease. *Circulation* 126: 975–990, 2012. doi:10.1161/CIRCULATIONAHA.111.085761.
25. **Guglin M, Khan H.** Pulmonary hypertension in heart failure. *J Card Fail* 16: 461–474, 2010. doi:10.1016/j.cardfail.2010.01.003.
26. **Haddad F, Hunt SA, Rosenthal DN, Murphy DJ.** Right ventricular function in cardiovascular disease, part I: Anatomy, physiology, aging, and functional assessment of the right ventricle. *Circulation* 117: 1436–1448, 2008. doi:10.1161/CIRCULATIONAHA.107.653576.
27. **Handoko ML, de Man FS, Happé CM, Schalij I, Musters RJ, Westerhof N, Postmus PE, Paulus WJ, van der Laarse WJ, Vonk-Noordegraaf A.** Opposite effects of training in rats with stable and progressive pulmonary hypertension. *Circulation* 120: 42–49, 2009. doi:10.1161/CIRCULATIONAHA.108.829713.
28. **Hansdottir S, Groskreutz DJ, Gehlbach BK.** WHO's in second?: A practical review of World Health Organization group 2 pulmonary hypertension. *Chest* 144: 638–650, 2013. doi:10.1378/chest.12-2114.
29. **Hasleton PS, Brooks NH.** Severe pulmonary vascular change in patients dying with right ventricular failure after heart transplantation. *Thorax* 50: 210–212, 1995. doi:10.1136/thx.50.2.210.
30. **Hassoun PM, Mouthon L, Barberà JA, Eddahibi S, Flores SC, Grimminger F, Jones PL, Maitland ML, Michelakis ED, Morrell NW, Newman JH, Rabinovitch M, Schermuly R, Stenmark KR, Voelkel NF, Yuan JX, Humbert M.** Inflammation, growth factors, and pulmonary vascular remodeling. *J Am Coll Cardiol* 54, *Suppl*: S10–S19, 2009. doi:10.1016/j.jacc.2009.04.006.
31. **Hentschel T, Yin N, Riad A, Habbazettl H, Weimann J, Koster A, Tschope C, Kuppe H, Kuebler WM.** Inhalation of the phosphodiesterase-3 inhibitor milrinone attenuates pulmonary hypertension in a rat model of congestive heart failure. *Anesthesiology* 106: 124–131, 2007. doi:10.1097/00000542-200701000-00021.
32. **Hsu S, Houston BA, Tampakakis E, Bacher AC, Rhodes PS, Mathai SC, Damico RL, Kolb TM, Hummers LK, Shah AA, McMahan Z, Corona-Villalobos CP, Zimmerman SL, Wigley FM, Hassoun PM, Kass DA, Tedford RJ.** Right Ventricular Functional Reserve in Pulmonary Arterial Hypertension. *Circulation* 133: 2413–2422, 2016. doi:10.1161/CIRCULATIONAHA.116.022082.
33. **Jasmin JF, Mercier I, Hnasko R, Cheung MW, Tanowitz HB, Dupuis J, Lisanti MP.** Lung remodeling and pulmonary hypertension after myocardial infarction: pathogenic role of reduced caveolin expression. *Cardiovasc Res* 63: 747–755, 2004. doi:10.1016/j.cardiores.2004.05.018.
34. **Jeffery TK, Morrell NW.** Molecular and cellular basis of pulmonary vascular remodeling in pulmonary hypertension. *Prog Cardiovasc Dis* 45: 173–202, 2002. doi:10.1053/pcad.2002.130041.
35. **Karatasakis GT, Karagounis LA, Kalyvas PA, Manginas A, Athanassopoulos GD, Aggelakas SA, Cokkinos DV.** Prognostic significance of echocardiographically estimated right ventricular shortening in advanced heart failure. *Am J Cardiol* 82: 329–334, 1998. doi:10.1016/S0002-9149(98)00344-0.
36. **Kelly RP, Ting CT, Yang TM, Liu CP, Maughan WL, Chang MS, Kass DA.** Effective arterial elastance as index of arterial vascular load in humans. *Circulation* 86: 513–521, 1992. doi:10.1161/01.CIR.86.2.513.
37. **Kerem A, Yin J, Kaestle SM, Hoffmann J, Schoene AM, Singh B, Kuppe H, Borst MM, Kuebler WM.** Lung endothelial dysfunction in congestive heart failure: role of impaired Ca^{2+} signaling and cytoskeletal reorganization. *Circ Res* 106: 1103–1116, 2010. doi:10.1161/CIRCRESAHA.109.210542.
38. **Kuehne T, Yilmaz S, Steendijk P, Moore P, Groenink M, Saaed M, Weber O, Higgins CB, Ewert P, Fleck E, Nagel E, Schulze-Neick I, Lange P.** Magnetic resonance imaging analysis of right ventricular pressure-volume loops: in vivo validation and clinical application in patients

with pulmonary hypertension. *Circulation* 110: 2010–2016, 2004. doi:10.1161/01.CIR.0000143138.02493.DD.

39. **Kumar D, Hacker TA, Buck J, Whitesell LF, Kaji EH, Douglas PS, Kamp TJ.** Distinct mouse coronary anatomy and myocardial infarction consequent to ligation. *Coron Artery Dis* 16: 41–44, 2005. doi:10.1097/00019501-200502000-00008.
40. **LaBourene JI, Coles JG, Johnson DJ, Mehra A, Keeley FW, Rabinovitch M.** Alterations in elastin and collagen related to the mechanism of progressive pulmonary venous obstruction in a piglet model. A hemodynamic, ultrastructural, and biochemical study. *Circ Res* 66: 438–456, 1990. doi:10.1161/01.RES.66.2.438.
41. **Lahm T, Frump AL, Albrecht ME, Fisher AJ, Cook TG, Jones TJ, Yakubov B, Whitson J, Fuchs RK, Liu A, Chesler NC, Brown MB.** 17β-Estradiol mediates superior adaptation of right ventricular function to acute strenuous exercise in female rats with severe pulmonary hypertension. *Am J Physiol Lung Cell Mol Physiol* 311: L375–L388, 2016. doi:10.1152/ajplung.00132.2016.
42. **Lam CS, Roger VL, Rodeheffer RJ, Borlaug BA, Enders FT, Redfield MM.** Pulmonary hypertension in heart failure with preserved ejection fraction: a community-based study. *J Am Coll Cardiol* 53: 1119–1126, 2009. doi:10.1016/j.jacc.2008.11.051.
43. **Linehan JH, Haworth ST, Nelin LD, Krenz GS, Dawson CA.** A simple distensible vessel model for interpreting pulmonary vascular pressure-flow curves. *J Appl Physiol (1985)* 73: 987–994, 1992. doi:10.1152/jappl.1992.73.3.987.
44. **Liu A, Hacker T, Eickhoff JC, Chesler NC.** Estrogen preserves pulsatile pulmonary arterial hemodynamics in pulmonary arterial hypertension. *Ann Biomed Eng* 45: 632–643, 2017. doi:10.1007/s10439-016-1716-1.
45. **Liu A, Schreier D, Tian L, Eickhoff JC, Wang Z, Hacker TA, Chesler NC.** Direct and indirect protection of right ventricular function by estrogen in an experimental model of pulmonary arterial hypertension. *Am J Physiol Heart Circ Physiol* 307: H273–H283, 2014. doi:10.1152/ajpheart.00758.2013.
46. **Lundgren J, Rådegran G.** Pathophysiology and potential treatments of pulmonary hypertension due to systolic left heart failure. *Acta Physiol (Oxf)* 211: 314–333, 2014. doi:10.1111/apha.12295.
47. **Malhotra R, Dhakal BP, Eisman AS, Pappagianopoulos PP, Dress A, Weiner RB, Baggish AL, Semigran MJ, Lewis GD.** Pulmonary vascular distensibility predicts pulmonary hypertension severity, exercise capacity, and survival in heart failure. *Circ Heart Fail* 9: e003011, 2016. doi:10.1161/CIRCHEARTFAILURE.115.003011.
48. **Mandegar M, Fung YC, Huang W, Remillard CV, Rubin LJ, Yuan JX.** Cellular and molecular mechanisms of pulmonary vascular remodeling: role in the development of pulmonary hypertension. *Microvasc Res* 68: 75–103, 2004. doi:10.1016/j.mvr.2004.06.001.
49. **Meng Q, Lai Y-C, Kelly NJ, Bueno M, Baust JJ, Bachman TN, Goncharov D, Vanderpool RR, Radder JE, Hu J, Goncharova E, Morris AM, Mora AL, Shapiro SD, Gladwin MT.** Development of a mouse model of metabolic syndrome, pulmonary hypertension, and heart failure with preserved ejection fraction. *Am J Respir Cell Mol Biol* 56: 497–505, 2017. doi:10.1165/rcmb.2016-0177OC.
50. **Miller WL, Grill DE, Borlaug BA.** Clinical features, hemodynamics, and outcomes of pulmonary hypertension due to chronic heart failure with reduced ejection fraction: pulmonary hypertension and heart failure. *JACC Heart Fail* 1: 290–299, 2013. doi:10.1016/j.jchf.2013.05.001.
51. **Mozaffarian D, Benjamin EJ, Go AS, Arnett DK, Blaha MJ, Cushman M, Das SR, de Ferranti S, Després JP, Fullerton HJ, Howard VJ, Huffman MD, Isasi CR, Jiménez MC, Judd SE, Kissela BM, Lichtman JH, Lisabeth LD, Liu S, Mackey RH, Magid DJ, McGuire DK, Mohler ER 3rd, Moy CS, Muntner P, Mussolino ME, Nasir K, Neumar RW, Nichol G, Palaniappan L, Pandey DK, Reeves MJ, Rodriguez CJ, Rosamond W, Sorlie PD, Stein J, Towfighi A, Turan TN, Virani SS, Woo D, Yeh RW, Turner MB; Writing Group Members; American Heart Association Statistics Committee; Stroke Statistics Subcommittee.** Heart Disease and Stroke Statistics-2016 Update: a report from the American Heart Association. *Circulation* 133: e38–e360, 2016. doi:10.1161/CIR.0000000000000350.
52. **Naeije R.** Pulmonary vascular resistance. A meaningless variable? *Intensive Care Med* 29: 526–529, 2003. doi:10.1007/s00134-003-1693-3.
53. **Naeije R, Vachiery JL, Yerly P, Vanderpool R.** The transpulmonary pressure gradient for the diagnosis of pulmonary vascular disease. *Eur Respir J* 41: 217–223, 2013. doi:10.1183/09031936.00074312.
54. **Nahrendorf M, Badea C, Hedlund LW, Figueiredo JL, Sosnovik DE, Johnson GA, Weissleder R.** High-resolution imaging of murine myocardial infarction with delayed-enhancement cine micro-CT. *Am J Physiol Heart Circ Physiol* 292: H3172–H3178, 2007. doi:10.1152/ajpheart.01307.2006.
55. **Nozawa T, Yasumura Y, Futaki S, Tanaka N, Uenishi M, Suga H.** Efficiency of energy transfer from pressure-volume area to external mechanical work increases with contractile state and decreases with afterload in the left ventricle of the anesthetized closed-chest dog. *Circulation* 77: 1116–1124, 1988. doi:10.1161/01.CIR.77.5.1116.
56. **Ontkean M, Gay R, Greenberg B.** Diminished endothelium-derived relaxing factor activity in an experimental model of chronic heart failure. *Circ Res* 69: 1088–1096, 1991. doi:10.1161/01.RES.69.4.1088.
57. **Pacher P, Nagayama T, Mukhopadhyay P, Bátkai S, Kass DA.** Measurement of cardiac function using pressure-volume conductance catheter technique in mice and rats. *Nat Protoc* 3: 1422–1434, 2008. doi:10.1038/nprot.2008.138.
58. **Pagnamenta A, Dewachter C, McEntee K, Fesler P, Brimioulle S, Naeije R.** Early right ventriculo-arterial uncoupling in borderline pulmonary hypertension on experimental heart failure. *J Appl Physiol (1985)* 109: 1080–1085, 2010. doi:10.1152/japplphysiol.00467.2010.
59. **Pereda D, García-Alvarez A, Sánchez-Quintana D, Nuño M, Fernández-Friera L, Fernández-Jiménez R, García-Ruíz JM, Sandoval E, Aguero J, Castellá M, Hajjar RJ, Fuster V, Ibáñez B.** Swine model of chronic postcapillary pulmonary hypertension with right ventricular remodeling: long-term characterization by cardiac catheterization, magnetic resonance, and pathology. *J Cardiovasc Transl Res* 7: 494–506, 2014. doi:10.1007/s12265-014-9564-6.
60. **Polak JF, Holman BL, Wynne J, Colucci WS.** Right ventricular ejection fraction: an indicator of increased mortality in patients with congestive heart failure associated with coronary artery disease. *J Am Coll Cardiol* 2: 217–224, 1983. doi:10.1016/S0735-1097(83)80156-9.
61. **Pradhan K, Sydykov A, Tian X, Mamazhakypov A, Neupane B, Luitel H, Weissmann N, Seeger W, Grimminger F, Kretschmer A, Stasch JP, Ghofrani HA, Schermuly RT.** Soluble guanylate cyclase stimulator riociguat and phosphodiesterase 5 inhibitor sildenafil ameliorate pulmonary hypertension due to left heart disease in mice. *Int J Cardiol* 216: 85–91, 2016. doi:10.1016/j.ijcard.2016.04.098.
62. **Provencher S, Archer SL, Ramirez FD, Hibbert B, Paulin R, Boucherat O, Lacasse Y, Bonnet S.** Standards and methodological rigor in pulmonary arterial hypertension preclinical and translational research. *Circ Res* 122: 1021–1032, 2018. doi:10.1161/CIRCRESAHA.117.312579.
63. **Ramu B, Thenappan T.** Evolving concepts of pulmonary hypertension secondary to left heart disease. *Curr Heart Fail Rep* 13: 92–102, 2016. doi:10.1007/s11897-016-0284-x.
64. **Reeves JT, Linehan JH, Stenmark KR.** Distensibility of the normal human lung circulation during exercise. *Am J Physiol Lung Cell Mol Physiol* 288: L419–L425, 2005. doi:10.1152/ajplung.00162.2004.
65. **Schreier D, Hacker T, Song G, Chesler N.** The role of collagen synthesis in ventricular and vascular adaptation to hypoxic pulmonary hypertension. *J Biomech Eng* 135: 021018, 2013. doi:10.1115/1.4023480.
66. **Silove ED, Tavernor WD, Berry CL.** Reactive pulmonary arterial hypertension after pulmonary venous constriction in the calf. *Cardiovasc Res* 6: 36–44, 1972. doi:10.1093/cvr/6.1.36.
67. **Stenmark KR, Davie N, Frid M, Gerasimovskaya E, Das M.** Role of the adventitia in pulmonary vascular remodeling. *Physiology (Bethesda)* 21: 134–145, 2006. doi:10.1152/physiol.00053.2005.
68. **Stenmark KR, Fagan KA, Frid MG.** Hypoxia-induced pulmonary vascular remodeling: cellular and molecular mechanisms. *Circ Res* 99: 675–691, 2006. doi:10.1161/01.RES.0000243584.45145.3f.
69. **Stenmark KR, Nozik-Grayck E, Gerasimovskaya E, Anwar A, Li M, Riddle S, Frid M.** The adventitia: Essential role in pulmonary vascular remodeling. *Compr Physiol* 1: 141–161, 2011. doi:10.1002/cphy.c090017.
70. **Tabima DM, Hacker TA, Chesler NC.** Measuring right ventricular function in the normal and hypertensive mouse hearts using admittance-derived pressure-volume loops. *Am J Physiol Heart Circ Physiol* 299: H2069–H2075, 2010. doi:10.1152/ajpheart.00805.2010.
71. **Tabima DM, Philip JL, Chesler NC.** Right Ventricular-Pulmonary Vascular Interactions. *Physiology (Bethesda)* 32: 346–356, 2017. doi:10.1152/physiol.00040.2016.
72. **Townsley MI.** Structure and composition of pulmonary arteries, capillaries, and veins. *Compr Physiol* 2: 675–709, 2012. doi:10.1002/cphy.c100081.
73. **Tuchscherer HA, Vanderpool RR, Chesler NC.** Pulmonary vascular remodeling in isolated mouse lungs: effects on pulsatile pressure-flow relationships. *J Biomech* 40: 993–1001, 2007. doi:10.1016/j.jbiomech.2006.03.023.

74. **Tuchscherer HA, Webster EB, Chesler NC.** Pulmonary vascular resistance and impedance in isolated mouse lungs: effects of pulmonary emboli. *Ann Biomed Eng* 34: 660–668, 2006. doi:10.1007/s10439-005-9050-z.
75. **Vachiéry JL, Adir Y, Barberà JA, Champion H, Coghlan JG, Cottin V, De Marco T, Galiè N, Ghio S, Gibbs JS, Martinez F, Semigran M, Simonneau G, Wells A, Seeger W.** Pulmonary hypertension due to left heart diseases. *J Am Coll Cardiol* 62, *Suppl*: D100–D108, 2013. doi:10.1016/j.jacc.2013.10.033.
76. **Vanderpool RR, Chesler NC.** Characterization of the isolated, ventilated, and instrumented mouse lung perfused with pulsatile flow. *J Vis Exp* 50: 2690, 2011. doi:10.3791/2690.
77. **Vanderpool RR, Naeije R, Chesler NC.** Impedance in isolated mouse lungs for the determination of site of action of vasoactive agents and disease. *Ann Biomed Eng* 38: 1854–1861, 2010. doi:10.1007/s10439-010-9960-2.
78. **Vonk-Noordegraaf A, Haddad F, Chin KM, Forfia PR, Kawut SM, Lumens J, Naeije R, Newman J, Oudiz RJ, Provencher S, Torbicki A, Voelkel NF, Hassoun PM.** Right heart adaptation to pulmonary arterial hypertension: physiology and pathobiology. *J Am Coll Cardiol* 62, *Suppl*: D22–D33, 2013. doi:10.1016/j.jacc.2013.10.027.
79. **Wang Z, Lakes RS, Golob M, Eickhoff JC, Chesler NC.** Changes in large pulmonary arterial viscoelasticity in chronic pulmonary hypertension. *PLoS One* 8: e78569, 2013. doi:10.1371/journal.pone.0078569.
80. **Wiesmann F, Frydrychowicz A, Rautenberg J, Illinger R, Rommel E, Haase A, Neubauer S.** Analysis of right ventricular function in healthy mice and a murine model of heart failure by in vivo MRI. *Am J Physiol Heart Circ Physiol* 283: H1065–H1071, 2002. doi:10.1152/ajpheart.00802.2001.
81. **Yu CM, Sanderson JE, Chan S, Yeung L, Hung YT, Woo KS.** Right ventricular diastolic dysfunction in heart failure. *Circulation* 93: 1509–1514, 1996. doi:10.1161/01.CIR.93.8.1509.